

Exciton spin dynamics in GaSe

Yanhao Tang,¹ Wei Xie,¹ Krishna C. Mandal,² John A. McGuire,^{1,*} and Chih-Wei Lai^{1,†}

¹*Department of Physics and Astronomy, Michigan State University, East Lansing, MI 48824, USA*
²*Department of Electrical Engineering, University of South Carolina, Columbia, SC 29208, USA*

We analyze exciton spin dynamics in GaSe under *nonresonant* circularly polarized optical pumping. Polarized time-dependent photoluminescence (PL) measurements reveals an initial circular polarization approaching unity even after dissipating more than 0.15 eV excess energy. The exciton spin relaxation times are deduced from the time-dependent PL circular polarization that exhibits a bi-exponential decay with a sub-20 ps and a >500 ps time constant. Spin relaxation of hot spin-polarized carriers nonresonantly optically injected into GaSe is dominated by the Elliot-Yafet spin-relaxation mechanism; a sub-20 ps spin relaxation time results. By contrast, the spin relaxation rate of cold excitons (*e-h* pairs) formed near the Γ point near the band edge is greatly reduced as a result of the suppressed D'yakonov-Perel' spin-relaxation mechanism. The separation of the non-degenerate conduction and valence bands from other bands result in angular momentum preservation for both electrons and holes.

I. INTRODUCTION

High spin polarization and long spin relaxation time in solid-state systems are desirable for many spintronic applications. Toward this goal, non-equilibrium spin dynamics has been investigated in various semiconductors¹⁻⁶, with gallium arsenide (GaAs) the most studied one. However, the the degenerate heavy- and light-hole valence bands and sub-ps hole spin relaxation in GaAs has limited optically pumped electron spin polarization in GaAs to 1/2 and the degree of circular polarization of resulting photoluminescence (PL) to 1/4^{1,2}. The *electron* spin relaxation times can be enhanced by doping⁷ or quantum confinement⁸. For example, near unity electron spin polarization can be obtained in heterostructures where heavy- and light-hole energy degeneracy is lifted by quantum confinement or strain⁹⁻¹¹.

In a recent report, we demonstrated that generation and preservation of a high degree of optical spin polarization, ρ , is possible in nanoscale slabs of GaSe even when optically pumping 0.1 to 0.2 eV above the gap¹². This is a consequence of the unique bandstructure (Fig. 1) of the group-III monochalcogenides^{13,14}, which consists of orbitally non-degenerate uppermost valence band (UVB) and lowermost conduction band (LCB) with minimal spin-orbit induced spin splittings¹⁵. Spin-flip processes in GaSe also result in polarized remote edge luminescence at the cleaved edges of GaSe platelets of about 150 nm or thicker through index-guiding¹⁶. In this study, we show that the exciton spin dynamics in GaSe at low temperature can be quantitatively reproduced by a simple model including momentum relaxation of excitons and spin relaxation of excitons and carriers.

II. CRYSTAL AND BAND STRUCTURES

The III-VI semiconducting compounds GaS, GaSe, and GaTe (MX) all form layered crystals. The bonding between the layers is weak, resulting in the easy cleav-

age of these crystals. In the case of GaS and GaSe, each layer consists of four planes of atoms in the sequence X-M-M-X and belong to the space group D_{3h}^1 . Different stacking orders of hexagonal layers result in formation of four commonly known polytypes: β (D_{6h}^4), ϵ (D_{3h}^1), rhombohedral γ (C_{3v}^5), and δ . Symmetry-dependent optical transitions and spin dynamics near the band edge can be sensitive to polytypes¹⁷. Here, we study ϵ -GaSe which has an ABA (Bernal) stacking order and belongs to space group $D_{3h}^1 - P\bar{6}m2$, which is noncentrosymmetric, i.e., lacking a spatial inversion center.

Bulk GaSe is generally regarded as an indirect band gap semiconductor. An indirect transition from the Γ to the M point \sim 10-20 meV below the direct gap at the Γ point is nearly resonant with the direct exciton transitions at the Γ point (exciton binding energy 20-30 meV)¹⁷⁻²⁵. Fig. 1 shows a schematic crystal structures and bandstructures of a bulk ϵ -GaSe. The LCB and UVB near the Γ point are derived primarily from Ga *s*-like and Se *p_z*-like orbitals and have respectively Γ_4 and Γ_1 symmetry. The valence bands are split by crystal-field anisotropy and spin-orbit interaction, leading to two bands with Se *p_x, p_y* symmetry about 1.2 and 1.6 eV below the UVB maximum.

The strongly anisotropic crystal structure leads to correspondingly anisotropic optical properties. The polarization vectors $\vec{E} \perp c$ and $\vec{E} \parallel c$ belong to the Γ_4 and Γ_6 representations, respectively. Considering the transition between uppermost valence band (Γ_1) and conduction band (Γ_4) without spin, the direct product $\Gamma_1 \times \Gamma_4$ belongs to the representation Γ_4 of D_{3h} ; therefore, the direct transition $\Gamma_1 \rightarrow \Gamma_4$ is orbitally allowed only for $\vec{E} \parallel c$. Taking into account spin, the direct transitions then occur between valence and conduction bands with the following symmetries in the double group \bar{D}_{3h} :

$$\begin{aligned} \Gamma_4 &\rightarrow \Gamma_8 \text{ (*s*-like conduction band)} \\ \Gamma_1 &\rightarrow \Gamma_7 \text{ (*B, p_z*-like valence band)} \\ \Gamma_5 &\rightarrow \Gamma_7 + \Gamma_9 \text{ (*A, p_{x,y}*-like valence band)} \\ \Gamma_6 &\rightarrow \Gamma_8 + \Gamma_9 \text{ (*C, p_{x,y}*-like valence band)} \end{aligned} \quad (1)$$

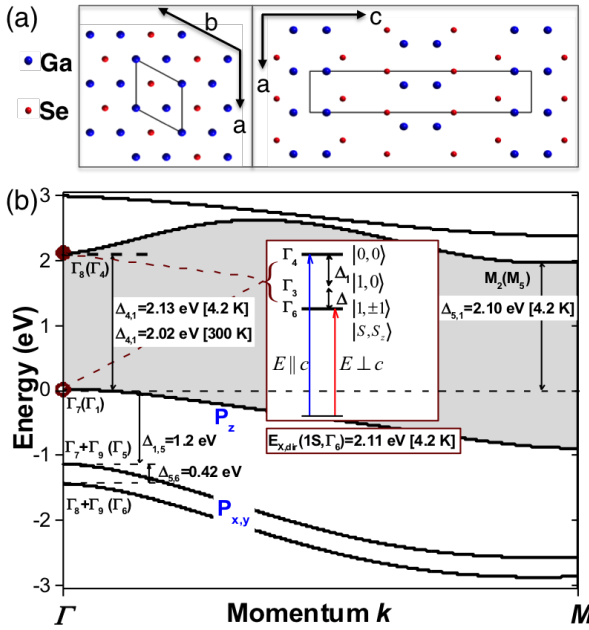


FIG. 1. Band structure and selection rules. (a) Crystal structure of ϵ -GaSe showing ABA stacking of the individual layers, space group $D_{3h}^1/P\bar{6}m2$ (#187) and point group D_{3h} . An individual layer consists of four planes of Se—Ga—Ga—Se, with the Ga—Ga bond normal to the layer plane arranged on a hexagonal lattice and the Se anions located in the eclipsed conformation when viewed along the c -axis. The inner solid boxes represent a unit cell. (b) Sketches of the band structure of ϵ -GaSe at the Γ point and the representations to which the states at the Γ -point belong with (without) spin-orbit interaction. (inset) Direct-gap excitons and selection rules.

The direct product $\Gamma_7 \times \Gamma_8 = \Gamma_3 + \Gamma_4 + \Gamma_6$ then contains the representations for both $\vec{E} \perp c$ and $\vec{E} \parallel c$. The optical transition between the UVB and LCB is dipole-allowed for $\vec{E} \parallel c$, whereas is only weakly allowed $\vec{E} \perp c$ because of spin-orbit coupling.

A complete accounting of the optical response requires an excitonic (two-particle) picture. To first approximation, one can regard band-edge excitons derived from carriers only in the conduction band and the Γ_1 UVB. This structure is then perturbed by spin-orbit mixing of the Γ_5 valence band into the UVB and then further perturbed by electron-hole exchange. The direct transition from the electronic ground state to an electron (Γ_8) and hole (Γ_7) in an s -like (Γ_1) direct-gap exciton state yields an exciton belonging to the following (degenerate) representations^{13,14,20,21,24}:

$$\Gamma_X^{(s)} = \Gamma_7 \times \Gamma_8 \times \Gamma_1 = \Gamma_4 + \Gamma_3 + \Gamma_6, \quad (2)$$

where Γ_4 is a pure spin singlet and Γ_3 and Γ_6 are pure spin triplet states.

Including spin-orbit mixing of the Γ_5 lower valence band into the UVB, the s -type band-edge excitonic wave-

functions become²⁰

$$\begin{aligned} \Gamma_4 &= |S\rangle + \alpha_4 |T\rangle, \\ \Gamma_3 &= |T\rangle, \\ \Gamma_6 &= |T\rangle + \alpha_6 |S\rangle, \end{aligned} \quad (3)$$

where $|S\rangle$ and $|T\rangle$ represent singlet and triplet states, respectively. Using Δ_{SO} measured by Sasaki et al.^{26,27}, the coefficients $\alpha_4 \approx \alpha_6 \approx (\Delta_{SO}/E_{BA}) \approx (0.44 \text{ eV}/1.27 \text{ eV}) \approx 0.35$. The Γ_5 state is mixed into the UVB at about the 10% level, consistent with the ratio of the oscillator strength (absorbance) between $\vec{E} \perp c$ and $\vec{E} \parallel c$. The upper level Γ_4 corresponds to a total exciton spin $S = 0$ and experiences a splitting $\Delta_1 \approx 2$ meV due to electron-hole exchange²⁰. The states Γ_3 and Γ_6 correspond to a total exciton spin $S = 1$, and $S_z = 0, \pm 1$ and are nearly degenerate (energy splitting $\Delta \approx 0$). These states are thus labeled by the indices 0 and ± 1 . The Γ_4 state can be excited by light with $\vec{E} \parallel c$. For optical excitation with wave vector $\vec{k} \parallel c$, Γ_6 ($S_z = \pm 1$) states can be excited by circularly polarized light with $\vec{E} \perp c$, whereas the Γ_3 state is optically inactive^{13,14}.

Earlier studies suggested a high degree of optical orientation in GaSe could be achieved under nearly resonant excitation at low temperatures. Through steady-state measurements, Gamarts et al.^{13,14} demonstrated optical orientation and alignment of excitons in GaSe by showing luminescence with circular polarization above 90% under steady-state circularly polarized optical excitation *in resonance* with direct excitons at cryogenic temperatures.

III. RESULTS

Sample preparation and experimental measurement methods were described previously¹². Thin films of GaSe crystals are mechanically exfoliated from a Bridgman-grown crystal²⁸ and deposited onto a silicon substrate with a 90 nm SiO_2 layer, with thickness measured by atomic force microscopy. Samples are mounted in vacuum on a copper cold finger attached to an optical liquid helium flow cryostat for all experiments. GaSe nanoslab are optically excited by 2 ps laser pulses from a synchronously pumped optical parametric oscillator ($\lambda_p \sim 560$ –595 nm, $E_p \sim 2.21$ –2.08 eV) or by second-harmonic pulses from a Ti:sapphire oscillator ($\lambda_p \sim 410$ nm, $E_p \sim 3.0$ eV). The laser beam is focused through a microscope objective (numerical aperture N.A. = 0.28) to an area of about $80 \mu\text{m}^2$ on the sample. The wave vector of the pump is along the crystal c -axis (the surface normal), i.e., the electric field vector \vec{E} is orthogonal to the c -axis ($\vec{E} \perp c$). The polarization and the flux (P) of the pump laser are controlled by liquid-crystal-based devices without mechanical moving parts. The samples are excited with the pump flux P from $0.1 P_0$ to P_0 , where $P_0 = 2.6 \times 10^{14} \text{ cm}^{-2}$ photons per pulse. We estimate the photoexcitation density to be from $\approx 2 \times 10^{16} \text{ cm}^{-3}$

to $3.4 \times 10^{17} \text{ cm}^{-3}$ ($2.7 \times 10^{-10} \text{ cm}^{-2}$ per layer) considering the absorption coefficient at 2.1 eV ($\approx 10^3 \text{ cm}^{-1}$ for $\vec{E} \perp c$) and Fresnel loss from reflection. The photoexcited carrier density is below the Mott transition²⁹ of direct excitons occurring near electron-hole (e - h) pair densities of $4 \times 10^{17} \text{ cm}^{-3}$.

Time- and polarization-resolved PL measurements allow us to separately determine the recombination time, the initial spin orientation, and the spin relaxation time. Polarized PL measurements are performed under excitation with excess energy about 0.1 to 0.2 eV above the exciton emission peak. The band-edge exciton PL emission at room temperature is near 620 nm (2.0 eV), independent of thickness. The exciton peak gradually red shifts from 590 nm (2.1 eV) to 620 nm (2.0 eV) in bulk ($> 1000 \text{ nm}$) to 90-nm nanoslabs at $T = 10 \text{ K}$. This shift is attributed to increasing contribution to PL from localized excitons, which is the subject of ongoing studies and beyond the scope of this paper. Additionally, we observe that the quantum yield of luminescence is greatly suppressed in sub-50-nm thick samples¹². In this paper, we focus on a 540 nm thick GaSe sample (S540nm). This sample is at the lower limit of the region in which we find surface trapping of carriers to play a negligible role in the sample properties.

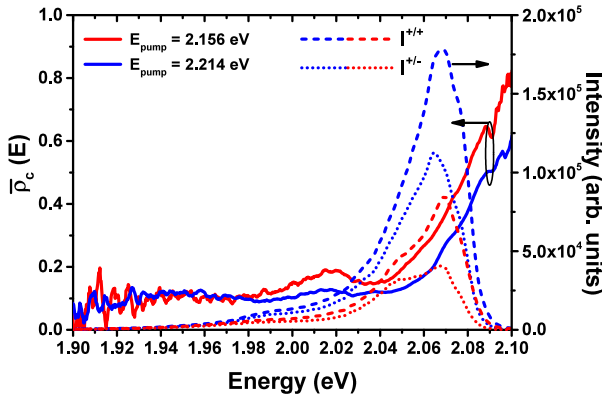


FIG. 2. **Polarized PL spectra under optical excitation at 2.156 eV and 2.214 eV.** Time-integrated PL spectra [$I^{+/+}(E)$ (co-circular, dashed lines) and $I^{+/-}(E)$ (cross-circular, dotted lines)] and degree of circular polarization $\bar{\rho}_c(E)$ (solid lines) of 540-nm thick (S540) GaSe samples under σ^+ excitation at pump flux $P = 0.5 P_0$, where $P_0 = 2.6 \times 10^{14} \text{ cm}^{-2}$ per pulse. Blue (Red) lines are for $E_{\text{pump}} = 2.214 \text{ eV}$ (2.156 eV).

Fig. 2 shows time-integrated PL spectra from a 540 nm-thick sample (S540nm) under co- and cross-circularly polarized excitation and detection at $T = 10 \text{ K}$. The PL is peaked at about 2.07 eV with a low-energy tail that is attributed to localized excitons. As in samples described previously¹², the degree of steady-state spin polarization ($\bar{\rho}_c$) is highest at high energies, as expected given the reduced time spent at such energies. There is also a pronounced increase in $\bar{\rho}_c$ as the excitation photon energy decreases towards the band gap. This is as expected from

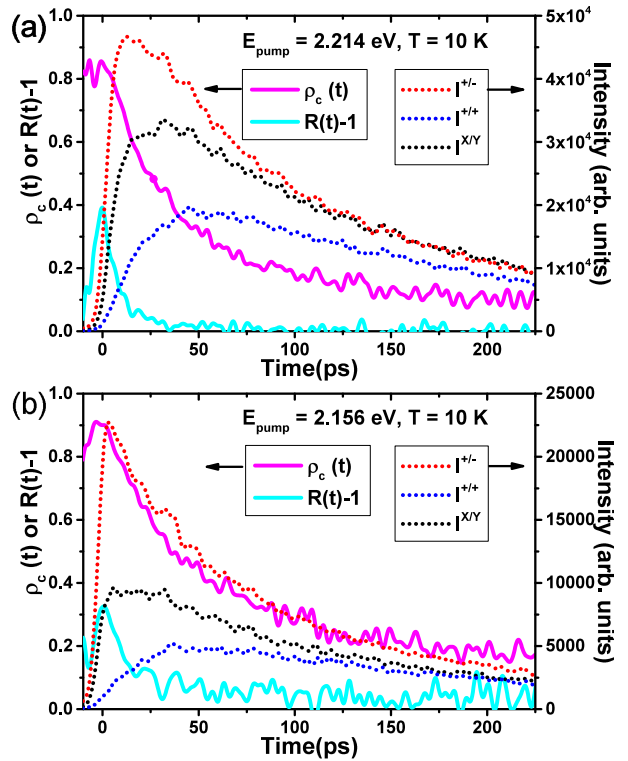


FIG. 3. **Polarized PL dynamics under optical excitation at 2.156 eV and 2.214 eV.** (a) Time-dependent PL intensity [$I^{+/-}(t)$, $I^{+/-}(t)$, and $I^{X/Y}(t)$ (dotted red, blue, and black, respectively)], degree of circular polarization $\rho_c(t)$ (solid magenta), and $R(t) - 1 = \frac{I^{+/-}(t) - I^{+/-}(t)}{I^{+/-}(t) + I^{+/-}(t)} - 1$ (solid cyan) under excitation $E_{\text{pump}} = 2.214 \text{ eV}$ at $P = 0.5 P_0$. (b) Same as (a), but for excitation $E_{\text{pump}} = 2.156 \text{ eV}$.

the greater spin-orbit field at larger k in the D'yakonov-Perel' mechanism of spin relaxation and the increased rate of scattering at larger k in the Elliott-Yafet mechanism.

For more direct insights into the nature of the spin relaxation, we perform time-resolved measurements of the spectrally integrated PL (Fig. 3). The PL at cryogenic temperatures (10 K) reveals a fast ($< 10 \text{ ps}$) rise time followed by a biexponential form with time constants $\tau'_0 \approx 20 - 50 \text{ ps}$ and $\tau''_0 \approx 150 - 200 \text{ ps}$ in all samples. The time-dependent circular polarization $\rho_c(t)$ is also observed to be biexponential with decay time constants $\tau'_s \approx 30 - 40 \text{ ps}$ and $\tau''_s \gtrsim 150 - 200 \text{ ps}$. The initial, resolution-limited rise in the PL signal represents the rate of carrier scattering to small values of the momentum (i.e., to near the band edge at the Γ point). The biexponential nature of $\rho_c(t)$ can be understood as a consequence of fast spin relaxation during thermalization to the band gap followed by slower spin relaxation once the carriers are at the band edge. The initial decay of spin po-

larization is greater at 2.156 eV than at 2.214 eV, again consistent with the expectation that greater spin-orbit field and faster momentum scattering at higher energies should result in faster spin relaxation.

Previously, we showed that carrier spin relaxation leads to rotation of the emission dipoles from in-plane to out-of-plane, i.e., from perpendicular to the c -axis to along the c -axis¹². This is manifested by the polarized remote edge luminescence (REL) at the cleaved edges of the sample as a result of idex-guided (waveguided) emission from out-of-plane dipoles¹⁶. Time-resolved measurements of the spectrally-integrated REL at $T = 10$ K reveal an initial rise of the REL with a ~ 30 ps timescale that matches the initial fast decay of the PL from the excitation spot.

IV. SPIN RELAXATION IN GROUP-III MONOCHALCOGENIDES

Spin relaxation mechanisms in semiconductors depend on detail in the energy versus momentum dispersion and spin-splitting due to spin-orbit interaction^{30,31}. In III-V semiconductors such as GaAs, the group-V p_x , p_y , and p_z -derived valence bands are closely spaced due to the small crystal field. Consequently, the angular momentum and quasimomentum of holes are strongly coupled, and the spin orientation of holes is lost in a period comparable to the momentum relaxation time (τ_p). The slower relaxation of *electron* spin in such semiconductors is a result of the reduced spin-orbit mixing of the group-III s -orbital-derived conduction band with distant bands. Electron spin relaxation is usually analyzed in terms of three mechanisms^{1,3,4,32}: D'yakonov-Perel' (DP), which is associated with spin-orbit-induced spin splitting of a band in noncentrosymmetric systems³³; Elliott-Yafet (EY)^{34,35}, which is associated with spin-orbit induced band-mixing; and Bir-Aronov-Pikus (BAP)³⁶⁻³⁹, which is associated with electron-hole exchange interactions.

Carrier spin relaxation depends on carrier energy because of increased spin-orbit coupling with increasing momentum and because of the influence of carrier energy on momentum scattering rates. The DP mechanism can be understood in terms of a momentum-dependent effective magnetic field so that for rapid momentum scattering motional narrowing results in a slowing of the decay of the spin polarization. Conversely, in the EY mechanism, momentum scattering is associated with a change of spin state during the scattering event, so that increasing momentum scattering results in rapid loss of spin polarization. Similarly, the momentum scattering time $\tau_p(n)$ is expected to decrease with increasing carrier density n . Therefore, the spin relaxation time, T_1 , should increase with increasing n if spin relaxation is dominated by the DP mechanism and decrease with increasing n if spin relaxation is dominated by the EY mechanism.

In comparison with GaAs which has $p_{x,y}$ -like UVBs, GaSe has a p_z -like UVB that is weakly coupled to other

energetically distant valence bands because of the large crystal field and spin-orbit coupling. This reduced mixing of valence band states in GaSe compared to III-V semiconductors should result in much slower EY-type hole spin relaxation than in, e.g., GaAs^{2,4,40-42}. For photoexcited carrier densities above 10^{16} cm⁻³ as studied in undoped GaSe here, we neglect spin relaxation due to the BAP mechanism. In our experiments, at $T = 10$ K, we found the initial decay of ρ_c is characterized by $\tau'_s \propto n^{-0.23}$. This suggests the EY mechanism plays a larger role than the DP mechanism in the initial spin relaxation in GaSe at low temperature.

When the electron (hole) lifetime is much longer than the energy relaxation time, the majority of electrons (holes) in the conduction (valence) band is thermalized under stationary excitation. Spin-momentum correlation is generally lost during thermalization. However, during the thermalization process and before the average spin polarization is completely lost, polarized *hot* photoluminescence may be observed. This can yield a higher degree of circular polarization at high energies in the steady-state spectrum. In GaSe, the initial carrier cooling to the band edge occurs in the sub-ps to sub-10 ps range (Fig. 3)⁴³. This fast energy and momentum relaxation (cooling) is demonstrated by the sub-10 ps PL rise time that is nearly independent of PL emission energy. Additionally, the PL decay is similar across the spectrum throughout the detection range (data not shown).

V. THEORETICAL MODELING

The dynamics of resonantly excited non-thermal excitons in quasi-two-dimensional systems such GaAs-based quantum-well structures are affected by several different physical processes^{42,44-45}: (1) momentum relaxation of excitons, (2) spin relaxation of excitons, and (3) the enhanced radiative recombination and propagation of exciton polaritons. For non-resonantly photo-excited carriers, one should also consider the contribution to dynamics from free carriers, in particular at high temperature. Here, we calculate the population of excitons in various spin and momentum states in GaSe as described in Sec. II using a simplified exciton spin-flip model (Fig. 4). The model is adapted from a unified model for resonantly excited excitons in GaAs-based quantum wells⁴⁷. In principle, this model should be valid only for resonant photoexcitation at low temperature where the contributions from free carriers is negligible. Nevertheless, we find that this model reproduces most of the present experimental photoluminescence polarization properties and dynamics.

We label exciton states as $|\pm\rangle \equiv |1, \pm\rangle$, $|1, 0\rangle$, and $|0, 0\rangle$. We first consider the case when the excitons are photoexcited in non-radiative, high-momentum states ($K_{\parallel} > K_0$) labelled, for example, $|+k\rangle$, where K_{\parallel} is the in-plane momentum of excitons and K_0 is the photon momentum. Exciton spin-flip (with rate W_X) transfers pop-

ulation between $|+\rangle$ and $|-\rangle$ states, while electron/hole spin-flip (indistinguishable for electron and hole in our experiments and so characterized by a single rate (W_s) populates the dipole-inactive $|1, 0\rangle$ non-radiative (dark) state, and the singlet $|0, 0\rangle$ state (dipole-active for $E \parallel c$). Following Vinattieri et al.⁴⁷, we divide the manifold of K_{\parallel} states into two sets, one for nearly zero K_{\parallel} and the other for finite large K_{\parallel} states. Each set includes the four exciton states. Absorption and emission of acoustic phonons induce transitions between these two sets. We consider only spin-conserving transitions with an effective scattering rate W_k . To simplify the model, we neglect any thermal factors associated with the spin-flip rates of excitons and electron/hole.

The time-dependent population in each state is given

by a set of coupled equations:

$$\frac{d}{dt} N_i = M_{ij} N_j + G(t) \delta_{+1k,i}, \quad (4)$$

where N_i is the column vector $(N_{+1}, N_{-1}, N_{10}, N_{00}, N_{+1k}, N_{-1k}, N_{10k}, N_{00k})$ and M is a 8×8 matrix. $N_{+1}, N_{-1}, N_{10}, N_{00}$ are populations of $K_{\parallel} \lesssim K_0$ states $|+\rangle, |-\rangle, |1, 0\rangle$, and $|0, 0\rangle$, respectively. $N_{+1k}, N_{-1k}, N_{10k}, N_{00k}$ are corresponding $K_{\parallel} > K_0$ states. M is the following matrix:

$$M = \begin{bmatrix} A & C \\ D & B \end{bmatrix}, \quad (5)$$

where A, B, C , and D are the following 4×4 matrices:

$$A = \begin{bmatrix} -(W_r + W_X + W_s + W_{kp}) & W_X & W_s/4 & W_s/4 \\ W_X & -(W_r + W_X + W_s + W_{kp}) & W_s/4 & W_s/4 \\ W_s/2 & W_s/2 & -(W_s/2 + W_{kp}) & 0 \\ W_s/2 & W_s/2 & 0 & -(W_r^0 + W_s/2 + W_{kp}) \end{bmatrix},$$

$$B = \begin{bmatrix} -(W_X + W_s + W_{km}) & W_X & W_s/4 & W_s/4 \\ W_X & -(W_X + W_s + W_{km}) & W_s/4 & W_s/4 \\ W_s/2 & W_s/2 & -(W_s/2 + W_{km}) & 0 \\ W_s/2 & W_s/2 & 0 & -(W_s/2 + W_{km}) \end{bmatrix},$$

$$C = \begin{bmatrix} W_{km} & 0 & 0 & 0 \\ 0 & W_{km} & 0 & 0 \\ 0 & 0 & W_{km} & 0 \\ 0 & 0 & 0 & W_{km} \end{bmatrix}, \quad D = \begin{bmatrix} W_{kp} & 0 & 0 & 0 \\ 0 & W_{kp} & 0 & 0 \\ 0 & 0 & W_{kp} & 0 \\ 0 & 0 & 0 & W_{kp} \end{bmatrix}.$$

W_r and W_r^0 are the radiative recombination rates for $|\pm 1/2\rangle$ and $|0, 0\rangle$, respectively. W_X and W_s are the exciton and electron/hole spin-relaxation rates. The acoustic-phonon scattering rates W_{kp} and W_{km} are defined by Vinattieri et al.⁴⁷ as

$$W_{kp} = W_k \exp \left[-\frac{\hbar \Gamma_h}{k_B T} \right],$$

$$W_{km} = W_k \left(1 - \exp \left[-\frac{\hbar \Gamma_h}{k_B T} \right] \right), \quad (6)$$

where W_k is the effective scattering rate with phonons, and $\hbar \Gamma_h$ is the homogeneous linewidth. The spin-flip rates of electrons and holes cannot be distinguished in this model because spin-flip of electron and holes results in identical transitions within the model.

There are six parameters in the model ($W_r^0, W_r, W_X, W_s, W_k, \Gamma_h$). However, the present and prior experimental data strongly constrain these rates so that we can obtain quantitative information about these rates by fitting the experimental polarized PL dynamics with this model (Fig. 4). The radiative recombination rate W_r^0 for state $|0, 0\rangle$ is set to 30 W_r based on the relative absorption coefficients between $E \parallel c$ and $E \perp c$ light²². The value of Γ_h

is not available but in principle can be measured independently from temperature-dependent PL linewidths^{55–58}. For simplicity, we set $\hbar \Gamma_h = k_B T$ because the linewidth increases from ~ 30 meV at $T = 10$ K to ~ 50 meV at $T = 300$ K. W_r is then largely determined by the decay of population (the measured PL decay).

We first consider the remote edge luminescence (REL) reported previously¹⁶. Excitation with light polarized perpendicular to c results in linearly polarized emission with polarization along the line from the excitation spot to the emission spot. This is due to scattering of the triplet-like excitons into the $|0, 0\rangle$ singlet-like exciton state. The initial rate of build up of the REL and corresponding initial rate of decay of the triplet emission from the focal spot correspond to the scattering rate W_s .

We next consider the total time-dependent PL under linearly and circularly polarized excitation conditions. Under linearly polarized excitation, the photoexcited electrons and holes are assumed to be equally distributed over their respective spin states, i.e. $|\pm 1/2\rangle$, during the initial 2-ps laser excitation. The non-geminate (bimolecular) formation of excitons then produces an initial exciton population distributed equally over the three triplet exciton states $|\pm\rangle$ and $|1, 0\rangle$. We con-

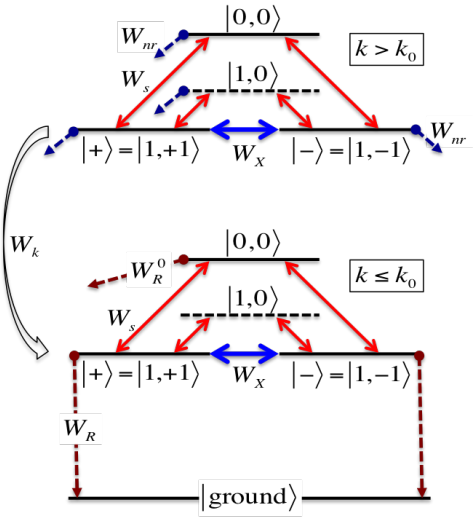


FIG. 4. Schematic of the model for the exciton dynamics.

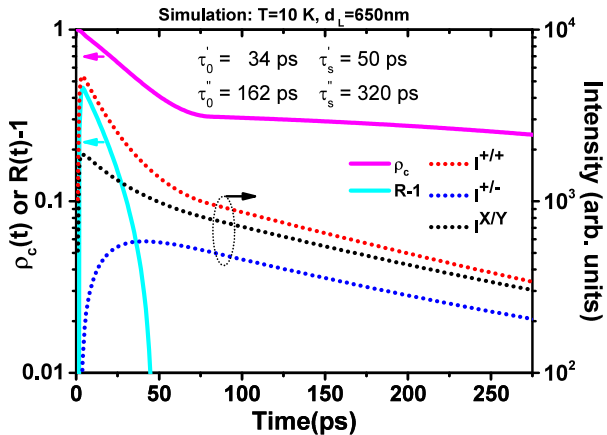


FIG. 5. Calculated polarized PL dynamics for $T = 10$ K and $d_L = 650$ nm.

trast this to the case of circularly polarized excitation (σ^+), under which only the bright exciton state $|+\rangle$ is initially formed. The total time-dependent populations of $|+\rangle$ and $|-\rangle$ created by circularly and linearly polarized light are labeled $I^+(t)$ and $I^X(t)$, respectively. Then the ratio $R(t) = I^+(t)/I^X(t) = [I^{+/+}(t) + I^{+/-}(t)] / [I^{X/X}(t) + I^{X/Y}(t)]$ will decrease from approximately 1.5 to 1 as the populations in the three triplet states eventually become nearly equal

through spin relaxation under σ^+ excitation.

In order to estimate W_X , we first focus on polarized PL dynamics under circularly polarized excitation. The sum of time-dependent σ^+ and σ^- PL under circularly polarized σ^\pm excitation and σ^X and σ^Y PL under linearly polarized $\sigma^{X/Y}$ excitation are both independent of W_X because W_X does not change the total population in the two radiative states. By fitting experimental results for the polarized and total (i.e., unpolarized) PL versus time, we find that polarized PL dynamics is dominated by W_s at cryogenic temperatures ($T = 10$ K). We note that polarized PL dynamics in GaAs-based quantum-well structures at cryogenic temperatures is either dominated by electron/hole spin flip or a combination of exciton exchange and single electron/hole spin flip.^{44,59}

The preceding discussion of the decay of spin polarization applies to band-edge carriers. However, it does not account for spin relaxation of carriers excited above the gap, which exhibit faster spin relaxation as they cool and scatter into the region $K_{\parallel} \leq K_0$.⁵⁴ At $T = 10$ K, the time-dependent degree of circular polarization ($\rho_c(t)$) exhibits bi-exponential decay. The corresponding time-dependent PL under linearly polarized excitation also decays bi-exponentially. Additionally, the ratio $R(t)$ decays to 1 within about 20 ps. We can account for these experimental features without appeal to the detailed non-equilibrium carrier distributions, by assigning a spin-flip rate that decreases linearly from about $W'_s \approx \alpha W_s$ to 1 W_s during the thermalization period τ_{th} . The thermalization time can be determined by fitting to the polarized PL dynamics at low temperature ($\tau_{th} \sim 80$ ps at $T = 10$ K). After including such phenomenological parameters $W'_s = 500 W_s$ and $\tau_{th} = 80$ ps in the model, we reproduce quantitatively $\rho_c(t)$, $I^{+/+}(t)$, $I^{+/-}(t)$, and $I^{X/Y}(t)$, and qualitatively $[R(t) - 1]$ (Fig. 5). The parameters used for calculations are as follows: $W_r = 0.006$ ps^{-1} , $W_{nr} < 10^{-4}$ ps^{-1} , $W_X < 10^{-5}$ ps^{-1} , $W_s = 0.001$ ps^{-1} , $W'_s = 0.5$ ps^{-1} , $\tau_{th} = 80$ ps, $\hbar\Gamma_h = 2$ meV, and $W_k = 1.0$ ps^{-1} . The calculated PL dynamics (Fig. 5) agree with the experimental results (Fig. 3).

ACKNOWLEDGMENTS

This work is supported by NSF grant DMR-09055944 and J. Cownen endowment at Michigan State University. This research has used the W. M. Keck Microfabrication Facility. We thank Brage Golding, Bhanu Mahanti, and Carlo Piermarocchi for comments and discussions.

* mcguire@pa.msu.edu

† cwlai@msu.edu

¹ M. I. Dyakonov and V. I. Perel', "Theory of optical spin orientation of electrons and nuclei in semiconductors," in *Optical Orientation, Modern Problems in Condensed Matter Sciences*, Vol. 8 (Elsevier, 1984) pp. 11–72.

² M. I. Dyakonov, ed., *Spin Physics in Semiconductors*, Springer Series in Solid-State Science, Vol. 157 (Springer, 2008).

³ G. E. Pikus and A. N. Titkov, "Spin relaxation under optical orientation in semiconductors," in *Optical Orientation, Modern Problems in Condensed Matter Sciences*, Vol. 8 (Elsevier, 1984) pp. 73–131.

- ⁴ M. W. Wu, J. H. Jiang, and M. Q. Weng, "Spin dynamics in semiconductors," *Phys. Rep.* **493**, 61 – 236 (2010).
- ⁵ I. Žutić, J. Fabian, and S. Das Sarma, "Spintronics: Fundamentals and applications," *Rev. Mod. Phys.* **76**, 323–410 (2004).
- ⁶ D. D. Awschalom, L. C. Bassett, A. S. Dzurak, E. L. Hu, and J. R. Petta, "Quantum spintronics: engineering and manipulating atom-like spins in semiconductors." *Science* **339**, 1174–9 (2013).
- ⁷ J. M. Kikkawa, I. P. Smorchkova, N. Samarth, and D. D. Awschalom, "Room-temperature spin memory in two-dimensional electron gases," *Science* **277**, 1284–1287 (1997).
- ⁸ Y. Ohno, R. Terauchi, T. Adachi, F. Matsukura, and H. Ohno, "Spin relaxation in GaAs(110) quantum wells," *Phys. Rev. Lett.* **83**, 4196–4199 (1999).
- ⁹ M. Kohl, M. R. Freeman, D. D. Awschalom, and J. M. Hong, "Femtosecond spectroscopy of carrier-spin relaxation in GaAs-Al_xGa_{1-x}As quantum wells," *Phys. Rev. B* **44**, 5923 (1991).
- ¹⁰ T. Amand, B. Dareys, B. Baylac, X. Marie, J. Barrau, M. Brousseau, D. J. Dunstan, and R. Planel, "Exciton formation and hole-spin relaxation in intrinsic quantum wells," *Phys. Rev. B* **50**, 11624–11628 (1994).
- ¹¹ S. Pfalz, R. Winkler, T. Nowitzki, D. Reuter, A. D. Wieck, D. Hägele, and M. Oestreich, "Optical orientation of electron spins in GaAs quantum wells," *Phys. Rev. B* **71**, 165305 (2005).
- ¹² Y. Tang, W. Xie, K. C. Mandal, J. A. McGuire, and C. W. Lai, "Near unity optical spin polarization in GaSe nanoslabs," [arXiv:1410.5523](https://arxiv.org/abs/1410.5523) (2014).
- ¹³ E. M. Gamarts, E. L. Ivchenko, M. I. Karaman, V. P. Mushinskii, G. E. Pikus, B. S. Razbirin, and A. N. Starukhin, "Optical orientation and alignment of free excitons in GaSe during resonance excitation. experiment," *Sov. Phys. JETP* **46**, 590 (1977).
- ¹⁴ E. L. Ivchenko, G. E. Pikus, B. S. Razbirin, and A. I. Starukhin, "Optical orientation and alignment of free excitons in GaSe under resonant excitation. theory." *Sov. Phys. JETP* **45**, 1172–1180 (1977).
- ¹⁵ D. T. Do, S. D. Mahanti, and C. W. Lai, "Spin splitting in 2D monochalcogenide semiconductors," [arXiv:1504.00725](https://arxiv.org/abs/1504.00725) (2015).
- ¹⁶ Y. Tang, W. Xie, K. C. Mandal, J. A. McGuire, and C. W. Lai, "Linearly polarized remote-edge luminescence in gase nanoslabs," [arXiv:1502.06070](https://arxiv.org/abs/1502.06070) (2015).
- ¹⁷ J. L. Brebner and E. Mooser, "Excitons in GaSe polytypes," *Phys. Lett. A* **24**, 274–275 (1967).
- ¹⁸ E. Aulich, J. L. Brebner, and E. Mooser, "Indirect energy gap in GaSe and GaS," *Phys. Status Solidi B* **31**, 129–131 (1969).
- ¹⁹ A. Mercier, E. Mooser, and J. P. Voitchovsky, "Near edge optical absorption and luminescence of GaSe, GaS and of mixed crystals," *J. Lumin.* **7**, 241 – 266 (1973).
- ²⁰ E. Mooser and M. Schlüter, "The band-gap excitons in gallium selenide," *Nuovo Cimento B* **18**, 164–208 (1973).
- ²¹ M. Schlüter, J. Camassel, S. Kohn, J. P. Voitchovsky, Y. R. Shen, and Marvin L. Cohen, "Optical properties of GaSe and GaS_xSe_{1-x} mixed crystals," *Phys. Rev. B* **13**, 3534–3547 (1976).
- ²² R. Le Toullec, N. Piccioli, M. Mejatty, and M. Balkanski, "Optical constants of ϵ -GaSe," *Nuovo Cimento B* **38**, 159–167 (1977).
- ²³ R. Le Toullec, N. Piccioli, and J. C. Chervin, "Optical properties of the band-edge exciton in GaSe crystals at 10 K," *Phys. Rev. B* **22**, 6162 (1980).
- ²⁴ Y. Sasaki and Y. Nishina, "Photoluminescence studies of indirect bound excitons in ϵ -GaSe," *Phys. Rev. B* **23**, 4089–4096 (1981).
- ²⁵ V. Capozzi, L. Pavesi, and J. L. Staehli, "Exciton-carrier scattering in gallium selenide," *Phys. Rev. B* **47**, 6340–6349 (1993).
- ²⁶ Y. Sasaki, C. Hamaguchi, and J. Nakai, "Electroreflectance of GaSe. I. Around 3.4 eV," *J. Phys. Soc. Jpn.* **38**, 162–168 (1975).
- ²⁷ Y. Sasaki, C. Hamaguchi, and J. Nakai, "Electroreflectance of GaSe. II. 3.5–4.1 eV region," *J. Phys. Soc. Jpn.* **38**, 169–174 (1975).
- ²⁸ K. C. Mandal, A. Mertiri, G. W. Pabst, R. G. Roy, Y. Cui, P. Battacharya, M. Groza, A. Burger, A. M. Conway, and R. J. Nikolic, "Layered III-VI chalcogenide semiconductor crystals for radiation detectors," in *Proc. SPIE*, Vol. 7079 (2008) p. 70790.
- ²⁹ L. Pavesi, J. L. Staehli, and V. Capozzi, "Mott transition of the excitons in GaSe," *Phys. Rev. B* **39**, 10982–10994 (1989).
- ³⁰ J. M. Luttinger and W. Kohn, "Motion of electrons and holes in perturbed periodic fields," *Phys. Rev.* **97**, 869 (1955).
- ³¹ E. O. Kane, "Band structure of indium antimonide," *J. Phys. Chem. Solids* **1**, 249–261 (1957).
- ³² P. Boross, B. Dóra, A. Kiss, and F. Simon, "A unified theory of spin-relaxation due to spin-orbit coupling in metals and semiconductors," *Sci. Rep.* **3**, 3233 (2013).
- ³³ M. I. D'yakonov and V. I. Perel', "Spin relaxation of conduction electrons in noncentrosymmetric semiconductors," *Sov. Phys. Solid State* **13**, 3023–3026 (1972).
- ³⁴ R. J. Elliott, "Theory of the effect of spin-orbit coupling on magnetic resonance in some semiconductors," *Phys. Rev.* **96**, 266–279 (1954).
- ³⁵ Y. Yafet, "g factors and spin-lattice relaxation of conduction electrons," in *Solid State Physics*, Solid State Physics, Vol. 14 (Academic Press, 1963) pp. 1–98.
- ³⁶ G. L. Bir and G. E. Pikus, "Optical orientation of excitons in uniaxial crystals. Large exchange splitting," *Sov. Phys. JETP* **37**, 1116 (1973).
- ³⁷ G. E. Pikus and G. L. Bir, "Optical orientation of excitons in cubic crystals," *Sov. Phys. JETP* **40**, 390–395 (1974).
- ³⁸ G. L. Bir, A. G. Aronov, and G. E. Pikus, "Spin relaxation of electrons due to scattering by holes," *Sov. Phys. JETP* **42**, 705–712 (1975).
- ³⁹ A. G. Aronov, G. E. Pikus, and A. N. Titkov, "Spin relaxation of conduction electrons in p-type III-V compounds," *Sov. Phys. JETP* **57**, 680 (1983).
- ⁴⁰ G. Fishman and G. Lampel, "Spin relaxation of photoelectrons in p-type gallium arsenide," *Phys. Rev. B* **16**, 820 (1977).
- ⁴¹ K. Zerrouati, F. Fabre, G. Bacquet, J. Bandet, J. Frandon, G. Lampel, and D. Paget, "Spin-lattice relaxation in p-type gallium arsenide single crystals," *Phys. Rev. B* **37**, 1334–1341 (1988).
- ⁴² T. Amand and X. Marie, "Exciton spin dynamics in semiconductor quantum wells," in *Spin Physics in Semiconductors*, edited by M. I. Dyakonov (Springer, 2008) pp. 55–89.
- ⁴³ S. Nusse, P. Haring Bolivar, H. Kurz, V. Klimov, and F. Levy, "Carrier cooling and exciton formation in GaSe," *Phys. Rev. B* **56**, 4578–4583 (1997).
- ⁴⁴ T. C. Damen, L. Viña, J. E. Cunningham, J. Shah, and

- L. J. Sham, "Subpicosecond spin relaxation dynamics of excitons and free carriers in GaAs quantum wells," *Phys. Rev. Lett.* **67**, 3432–3435 (1991).
- ⁴⁵ L. J. Sham, "Spin relaxation in semiconductor quantum wells," *J. Phys.: Condens. Matter* **5**, A51 (1993).
- ⁴⁶ M. Z. Maialle, E. A. de Andrada e Silva, and L. J. Sham, "Exciton spin dynamics in quantum wells," *Phys. Rev. B* **47**, 15776–15788 (1993).
- ⁴⁷ A. Vinattieri, J. Shah, T. C. Damen, D. S. Kim, L. N. Pfeiffer, M. Z. Maialle, and L. J. Sham, "Exciton dynamics in GaAs quantum wells under resonant excitation," *Phys. Rev. B* **50**, 10868 (1994).
- ⁴⁸ H. Wang, J. Shah, T. C. Damen, and L. N. Pfeiffer, "Spontaneous emission of excitons in GaAs quantum wells: the role of momentum scattering," *Phys. Rev. Lett.* **74**, 3065–3068 (1995).
- ⁴⁹ L. Muñoz, E. Pérez, L. Viña, and K. Ploog, "Spin relaxation in intrinsic GaAs quantum wells: Influence of excitonic localization," *Phys. Rev. B* **51**, 4247–4257 (1995).
- ⁵⁰ B. Baylac, T. Amand, M. Brousseau, X. Marie, B. Dareys, G. Bacquet, J. Barrau, and R. Planel, "Exciton spin relaxation in the 2D dense excitonic phase: the role of exchange interaction," *Semicon. Sci. Technol.* **10**, 295 (1995).
- ⁵¹ E. L. Ivchenko, "Spectroscopy of spin-polarized excitons in semiconductors," *Pure and Appl. Chem.* **67**, 463–463 (1995).
- ⁵² T. Amand, D. Robart, X. Marie, M. Brousseau, P. Le Jeune, and J. Barrau, "Spin relaxation in polarized interacting exciton gas in quantum wells," *Phys. Rev. B* **55**, 9880 (1997).
- ⁵³ P. Le Jeune, X. Marie, T. Amand, F. Romstad, F. Perez, J. Barrau, and M. Brousseau, "Spin-dependent exciton-exciton interactions in quantum wells," *Phys. Rev. B* **58**, 4853–4859 (1998).
- ⁵⁴ L. Viña, "Spin relaxation in low-dimensional systems," *J. Phys.: Condens. Matter* **11**, 5929 (1999).
- ⁵⁵ J. Feldmann, G. Peter, E. O. Göbel, P. Dawson, K. Moore, C. Foxon, and R. J. Elliott, "Linewidth dependence of radiative exciton lifetimes in quantum wells," *Phys. Rev. Lett.* **59**, 2337–2340 (1987).
- ⁵⁶ V. Srinivas, J. Hryniwicz, Y. J. Chen, and C. E. C. Wood, "Intrinsic linewidths and radiative lifetimes of free excitons in GaAs quantum wells," *Phys. Rev. B* **46**, 10193–10196 (1992).
- ⁵⁷ D. S. Citrin, "Radiative lifetimes of excitons in quantum wells: Localization and phase-coherence effects," *Phys. Rev. B* **47**, 3832–3841 (1993).
- ⁵⁸ J. Aaviksoo, "Time-resolved studies of excitonic polaritons," *J. Lumin.* **48** & **49**, 57–66 (1991).
- ⁵⁹ S. Bar-Ad and I. Bar-Joseph, "Exciton spin dynamics in GaAs heterostructures," *Phys. Rev. Lett.* **68**, 349–352 (1992).